# Supplemental Material for
# Mirror symmetry broken of sound vortex transmission in a single passive metasurface via phase coupling

Yugan Tang[1], Boyang Xie[1], Hui Liu[1], Ya Zhang[1], Hua Cheng[1],* and Shuqi Chen[1,2,3]†

[1] *The Key Laboratory of Weak Light Nonlinear Photonics, Ministry of Education, School of Physics and TEDA Institute of Applied Physics, Nankai University, Tianjin 300071, China*

[2] *School of Materials Science and Engineering, Smart Sensing Interdisciplinary Science Center, Nankai University, Tianjin 300350, China and*

[3] *The collaborative Innovation Center of Extreme Optics, Shanxi University, Taiyuan, Shanxi 030006, China*

### A. The mirror symmetry induced by symmetric transmission properties of unit cells.

To demonstrate the significance of the transmission-reflection phase coupling (TRPC) mechanism, we considered the unit cells of a traditional phase gradient metasurface (PGM) with full transmission. They possess the same resonator sections as the transmission-reflection-integrated (TRI) PGM, as shown in Fig. S1(a). The radius of waveguide is $R = 6.4$ cm. The azimuthal cross-section of the unit cell comprises four identical rows with a radial height of $h = R/4$. The wall and neck of the Helmholtz cavity have a thickness of 1.5 mm. The height ratio $h_0/h$ is 0.02, 0.362 and 0.455 for cell 1, 2 and 3, respectively. The perforated panel sections are removed in the PGM. The transmission phase difference between adjacent unit cells is $\Delta\varphi_t = -2\pi/3$, while the transmissivity is close to $T_a = 1$. The intrinsic transmission topological charge of the PGM is still $l_t^\xi = -2$. Owing to the 180° rotation of the coordinate system following the incident direction from forward to backward, the mirror-symmetric incident cases with $l_i^b = -l_i^f$ are essentially equivalent. Since the symmetric transmission properties for opposite incidences are inherent in reciprocity, the phase twists generated by the traditional PGM are fixed and mirror-symmetric. The corresponding transmitted vortices will also be mirror-symmetric as $l_t^f = l_i^f + l_t^\xi$ and $l_t^b = l_i^b - l_t^\xi = -l_t^f$. When the transmitted vortex exceeds the maximum order, the wave travelling in the PGM will experience MIRs with $L > 1$. However, unlike the proposed TRI PGM, the traditional PGM cannot provide an intrinsic reflection topological charge, and the coupled processes cannot happen due to the zero reflectivity $R_a = 0$. The equivalent phase difference accumulated only by the transmission phase with $\Delta\phi = L\Delta\varphi_t - 2\pi q$ still provides mirror-symmetric equivalent phase twists. For example, when the vortex is incident on the PGM with $l_i^f = -1$ ($l_i^b = 1$) for forward (backward) direction, it cannot directly pass through due to $l_t^f = -1 - 2 = -3$ ($l_t^b = 1 + 2 = 3$) exceeding the maximum order $l_M = 2$. The propagation process of $L = 2$ can provide $\Delta\phi = 2 \times (-\frac{2\pi}{3}) + 2\pi = \frac{2\pi}{3}$ with an equivalent topological charge $l^D = 2$. The emergent vortices with topological charges $l_r^b = -(l_i^f + l^D) = -1$ ($l_r^f = -(l_i^b - l^D) = 1$) below $l_M = 2$ can be reflected with $l_r^b = -1$ ($l_r^f = 1$) for forward (backward) incidence, which are still mirror-symmetric. When the mirror-symmetric vortices irradiate onto the PGM with $l_i^f = 1$ ($l_i^b = -1$) for forward (back-

* Corresponding author: hcheng@nankai.edu.cn
† Corresponding author: schen@nankai.edu.cn

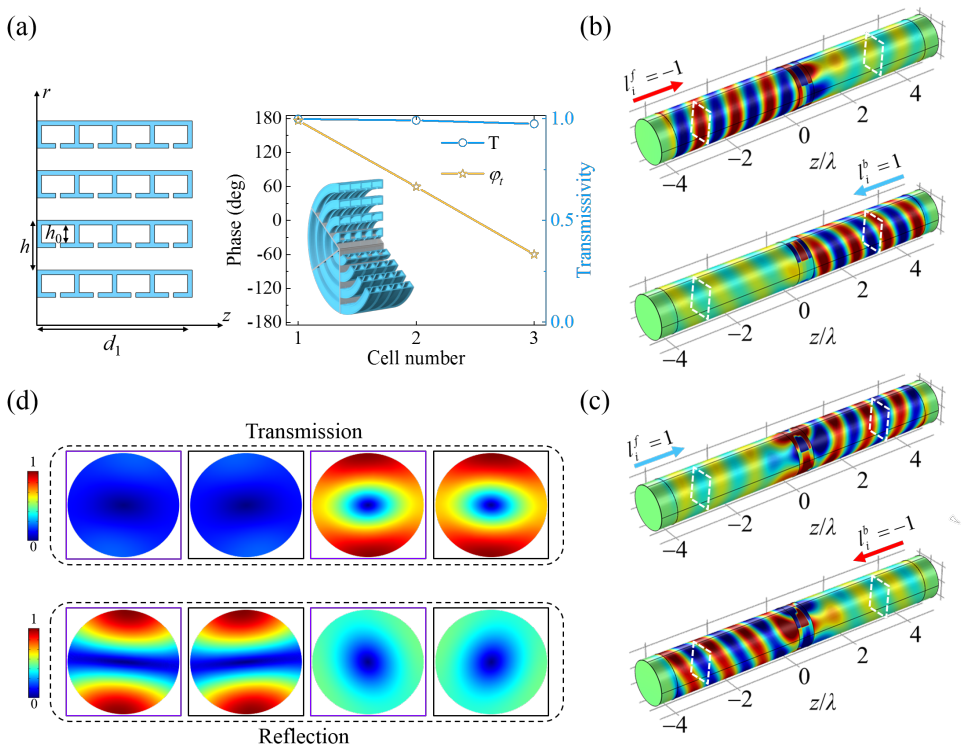


FIG. S1. Mirror-symmetric vortex generation via traditional PGM. (a) The PGM consists of six fanlike double-opening resonators with a length of $d_1 = 0.5\lambda$, and the parameters are consistent with those in the main text. The corresponding simulated transmission phase responses and transmission spectra for each unit cell are on the right. (b) and (c) The simulated scattered pressure fields for two pairs of mirror-symmetric incident vortices at 3430 Hz, with the PGM placed at $z = 0$. (d) The amplitude distributions of total pressure field patterns at $z = -2.6\lambda$ and $z = 3.1\lambda$. The amplitudes are normalized by the maximum values.

ward) direction, they will directly transmit in a mirror-symmetric way with $l_t^f = 1 - 2 = -1$ ($l_t^b = -1 + 2 = 1$). The simulated scattered pressure fields with incident vortices of $l_i^f = \pm 1$ and $l_i^b = \pm 1$ are delineated in Figs. S1(b) and S1(c). The total acoustic field distributions of the transmitted and reflected waves are shown in Fig. S1(d). These simulated results clearly validate the mirror symmetry properties induced by the fixed phase twists. The proposed TRPC mechanism in the TRI PGM makes it possible to produce disparate phase twists and achieve asymmetric transmission of mirror-symmetric vortex via a single passive PGM.

### B. The constitutive relation between phases.

By describing a single unit cell as a two-port system, the underlying relation between transmission and reflection phases can be expressed as [1]

$$2\varphi_t = \varphi_r + \varphi_{rB} + (2N+1)\pi, \tag{S1}$$

where $N$ is an integer. This relation is guaranteed by the reciprocity and conservation of energy. The phase difference between adjacent unit cells needs to satisfy

$$2\Delta\varphi_t = \Delta\varphi_r + \Delta\varphi_{rB} + 2\pi n, \tag{S2}$$

leading to

$$2l_t^{\xi} = l_r^{\xi} - l_{rB}^{\xi} + nM, \tag{S3}$$

where $n$ is an integer. The phase design of the TRI unit cells can be realized from Eq. (S2).

### C. Design procedure of perforated panel section.

In order to obtain the required reflection phase responses and simplify transmissivity control, we employed the perforated panel with length $d_2$ and aperture size $h_w$. The equivalent cross-section of the perforated panel is depicted schematically in Fig. S2(a), similar to the optical aperture. The plane wave is incident normally on the perforated panel along the $z$ direction with identical medium on both sides (i.e., medium I and III are the same). The transmission coefficient $t$ and reflection coefficient $r$ can be extracted as

$$t = \frac{2Z_{12}}{2Z_{12}\cos(k_z d_2) + i\left(1+{Z_{12}}^2\right)\sin(k_z d_2)}, \tag{S4}$$

$$r = \frac{i\left(1-{Z_{12}}^2\right)\sin(k_z d_2)}{2Z_{12}\cos(k_z d_2) + i\left(1+{Z_{12}}^2\right)\sin(k_z d_2)}, \tag{S5}$$

where $k_z = 2\pi/\lambda$ is the wave number in air and $Z_{12} = Z_1/Z_2 = h_w/R$ is the ratio of equivalent acoustic impedance. The scattering coefficients can also be expressed in another way with $t = |t|\, e^{i\varphi_t}$ and $r = |r|\, e^{i\varphi_r}$ [1]. Owing to the aperture size is smaller than the radius of the PGM with $h_w < R$ and $Z_{12} < 1$, $t = \frac{-i2Z_{12}}{\left(1+{Z_{12}}^2\right)}$ becomes a negative imaginary number and $r = \frac{1-{Z_{12}}^2}{1+{Z_{12}}^2}$ is a positive real number when $d_2 = \lambda/4$. The transmissivity can be modulated arbitrarily by changing $h_w$. The transmission and reflection phases remain

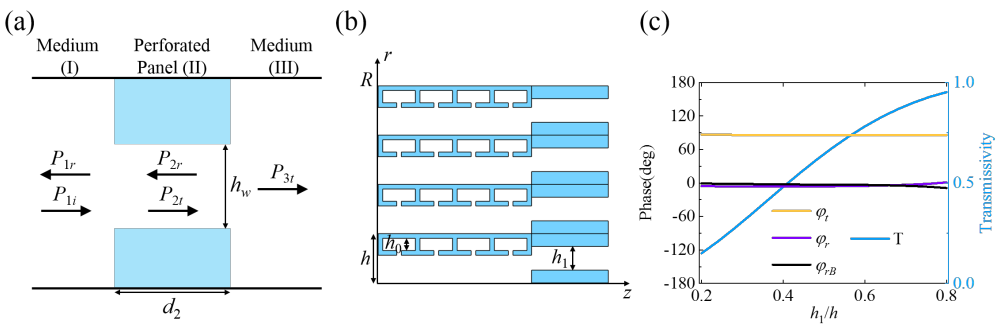


FIG. S2. (a) The equivalent medium view of the perforated panel. (b) Schematic cross-section of the cell 1. (c) The simulated transmission and reflection phase responses and transmission spectra of cell 1 as a function of $h_1$. The unit cell with perforated panel can provide constant transmission and reflection phases while modulating transmissivity.

constant and equal to $-\pi/2$ and 0, respectively, regardless of $h_w$. By introducing a perforated panel with $d_2 = \lambda/4$ behind the designed resonator section [see Fig. S2(b)], we can achieve the required reflection phase $\varphi_{rB} = 0$ for backward incidence and transmissivity $T_a = 0.5$ without affecting the transmission phase difference $\Delta\varphi_t = -2\pi/3$ between adjacent unit cells. In addition, the reflection phase difference $\Delta\varphi_r = 2\pi/3$ for forward incidence is guaranteed by Eq. (S2). Taking cell 1 of the TRI PGM as an example, the perforated panel with an aperture size $h_1$ consists of two blocks in each row. By changing $h_1$, we can find that the transmission and reflection phase responses are nearly constant over the entire parameter range in Fig. S2(c), which proves the ability of the perforated panel. Meanwhile, the type of perforated panel does not affect the phase and transmission responses [2, 3]; however, the cavity of resonator section with high ratio $h_0/h$ will make the channel stagger with the aperture of perforated panel, forming a mutated interface that affects the phase responses. The type of perforated panel can be optimized through simulation methods. Therefore, for cell 2 and 3 with high $h_0/h$, we designed the perforated panel with one block in each row to ensure continuous channels at the interface, as shown in Fig. 2(b). The corresponding designed aperture sizes $h_1$ for cell 1, 2 and 3 are $0.41h$, $0.39h$ and $0.365h$ per row, respectively.

### D. Details of simulations.

Three-dimensional (3D) full-wave simulations are implemented using the commercial software COMSOL Multiphysics 5.6a. The pressure-acoustic module with frequency domain research is employed, where the background pressure filed is used to generate incident vortex. The background medium is air with mass density $\rho = 1.2$ kg/m$^3$ and speed of sound $c = 343.2$ m/s. The materials of 3D PGM samples are set with $\rho = 1180$ kg/m$^3$ and $c = 2700$ m/s. A rigid cylindrical waveguide is used to explore the properties of the single PGM, with perfectly matched layers placed at the front and back. For investigating the phase responses and transmission spectra of the resonator unit cells, a two-dimensional (2D) pressure-acoustic module is utilized, assuming the walls to be sound-hard materials. Since the PGM, comprising fanlike resonator unit cells, is designed from a 2D approximation, there might be some tiny undesired scattering in the results, which can be improved by designing fanlike resonators in a 3D manner.

### E. The process of the topological charge conversions.

As shown in procedure ① of Fig. 2(d), when a vortex with topological charge $l_i^f = -1$ is incident forward, the sound wave will transmit and be reflected simultaneously. The topological charge of the reflected part is $l_r^b = -(l_i^f + l_r^\xi) = -1$, which is bellow the maximum topological charge $l_M = 2$ in the waveguide. Thus, it can leave the structure through a single reflection process of $L = L_r = 1$ (see the purple arrows). The reflectivity of this part of the reflected vortex is $R = R_a = 0.5$ and the topological charge is $l_r^b = -1$. For the transmitted part, because the total topological charge $l_t^f = l_i^f + l_t^\xi = -3$ exceeding the maximum order $l_M = 2$, it cannot exit the structure through a single transmission process of $L = L_t = 1$. Instead, it will undergo MIRs inside the PGM and go through the process of $L = 2$, including normal process of $L = L_t = 2$ and coupled process of $L = L_t + L_{rB} = 2$ ($L_t = 1$ and $L_{rB} = 1$). For the normal process, based on Eq. (1) in the main text, the equivalent phase difference between adjacent unit cells is $\Delta\phi = L_t\Delta\varphi_t - 2\pi q = 2\Delta\varphi_t + 2\pi = 2\pi/3$ ($\Delta\varphi_t = -2\pi/3$, $L_t = 2$, $q = -1$), leading to an equivalent topological charge $l^D = 2$. The total topological charge is $l_r^b = -(l_i^f + l^D) = -1$, which is less than the maximum order $l_M = 2$. Consequently, it can leave the PGM as a reflected vortex (see Eq. (3) in the main

text: $L_t$ is even) with reflectivity $R = {T_a}^2 = 0.25$ and topological charge $l_r^b = -1$. For the coupled process of $L = L_t + L_{rB} = 2$, the equivalent phase difference between adjacent unit cells is $\Delta\phi = \Delta\varphi_t + \Delta\varphi_{rB} = -2\pi/3$ ($\Delta\varphi_t = -2\pi/3$ and $\Delta\varphi_{rB} = 0$), providing $l^D = l_t^\xi = -2$. The total topological charge is $l_t^f = l_i^f + l^D = -3$, exceeding the maximum order $l_M = 2$. Thus, it is still forbidden to leave the PGM and will experience the next internal reflection with $L = 3$. The coupled process of $L = L_t + L_{rB} = 3$ includes two processes. One process is $L_t = 2$ and $L_{rB} = 1$ and another process is $L_t = 1$ and $L_{rB} = 2$. The former process is similar to $L_t = 2$ with $\Delta\phi = 2\Delta\varphi_t + \Delta\varphi_{rB} = 2\pi/3$ and $l^D = 2$, resulting in vortex reflection with $R = {T_a}^2 R_a = 0.125$ and $l_r^b = -1$. The latter process with $\Delta\phi = \Delta\varphi_t + 2\Delta\varphi_{rB} = -2\pi/3$ and $l^D = -2$ is still forbidden, while the coupled process of $L = 4$ will happen and so forth. By all processes considered, it can be concluded that when the vortex with topological charge $l_i^f = -1$ is incident forward, all transmission is prohibited, resulting in total reflected vortices with topological charge of $-1$ and reflectivity of 1.

When the mirror-symmetric vortex with $l_i^b = -1$ is incident backward, as shown in procedure ② of Fig. 2(d), the sound wave will also transmit and be reflected simultaneously. The topological charge $l_r^f = -(l_i^b + l_{rB}^\xi) = -1$ of the reflected vortex is below the maximum topological charge $l_M = 2$. Thus, it can leave the structure through a single reflection process of $L = L_{rB} = 1$ (see the black arrows) with reflectivity $R = R_a = 0.5$ and topological charge $l_r^f = -1$. For the transmitted vortex, the topological charge twisted by the PGM is $l_t^b = l_i^b - l_t^\xi = 3$ exceeding the maximum order. Therefore, it is forbidden to leave the structure via a single transmission process of $L = L_{tB} = 1$. Instead, it will go through the process of $L = 2$, including normal process of $L = L_{tB} = 2$ and coupled process of $L = L_{tB} + L_r = 2$ ($L_{tB} = 1$ and $L_r = 1$). For the normal process, it is mirror-symmetric to the forward incident case in procedure ① of Fig. 2(d), providing the same equivalent phase difference $\Delta\phi = L_{tB}\Delta\varphi_{tB} - 2\pi q = 2\pi/3$ between adjacent unit cells, resulting in an equivalent topological charge $l^D = 2$. The topological charge of the vortex twisted by the PGM is $l_r^f = -(l_i^b - l^D) = 1$, which is less than the maximum order. It can leave the PGM as a reflected vortex with reflectivity $R = {T_a}^2 = 0.25$ and topological charge $l_r^f = 1$. For the coupled process of $L = L_{tB} + L_r = 2$, it is different from procedure ① in Fig. 2(d). Owing to the designed asymmetric reflection phase differences $\Delta\varphi_r \neq \Delta\varphi_{rB}$, there exists an equivalent phase difference $\Delta\phi = \Delta\varphi_{tB} + \Delta\varphi_r = 0$ between adjacent unit cells, leading to $l^D = 0$. Benefiting from TRPC, the topological charge of vortex is $l_t^b = l_i^b + l^D = 1$ and

below the maximum order. Therefore, it will leave the PGM in a transmission way with transmissivity $T = T_a R_a$ and topological charge $l_t^b = 1$. By combining procedures ① and ②, the introduction of asymmetric reflection phase differences in TRPC can achieve one-way transmission of mirror-symmetric vortices.

Another pair of mirror-symmetric incident vortices with $l_i^f = 1$ for forward and $l_i^b = -1$ for backward direction are shown in procedures ③ and ④ of Fig. 2(e). By employing the similar discussions as above, asymmetric transmission with different topological charges can be achieved. As shown in procedure ③, part of the forward incident vortex is reflected with reflectivity $R = {R_a}^2 = 0.25$ and topological charge $l_r^b = 1$, while the transmitted vortices comprise two parts. One part experiences the coupled process of $L = L_r + L_t = 2$ ($L_r = 1$ and $L_t = 1$) and transmits with transmittivity $T = R_a T_a = 0.25$ and topological charge $l_t^f = 1$. The other part directly exits with transmittivity $T = T_a = 0.5$ and topological charge $l_t^f = l_i^f + l_t^\xi = -1$. For the backward incidence shown in procedure ④, there is no coupled process happening. Part of the vortex is directly reflected with reflectivity $R = R_a = 0.5$ and topological charge $l_r^f = -(l_i^b + l_{rB}^\xi) = 1$, while another part immediately transmits with transmittivity $T = T_a = 0.5$ and topological charge $l_t^b = l_i^b - l_t^\xi = 1$. Although the vortex transmission of the normal processes remain mirror-symmetric, the TRPC mechanism offers an extra transmission channel to support distinct transmission phase twists.

### F. The asymmetric transmissivities of vortex generated by the TRI PGM.

To quantify the asymmetric transmission of mirror-symmetric incident vortices, we mainly discuss the transmissivities (ratio of the outgoing to incoming sound power in the z direction) in this section. In theoretical prediction, the transmissivities are 0, 0.25, 0.75 and 0.5 for $l_i^f = -1$, $l_i^b = 1$, $l_i^f = 1$ and $l_i^b = -1$ at 3430 Hz, respectively. Figures. S3(a) and S3(b) show the corresponding simulated results with transmissivities of 0.013, 0.215, 0.605 and 0.404, which are in good agreement with the prediction at 3430 Hz. The frequency band of asymmetric transmission spans approximately 20 Hz (3420∼3440 Hz), demonstrating the disparate phase twists generated by the proposed TRI PGM. Theoretical analysis [see Figs. 2(d) and 2(e)] indicates that the topological charge proportions for transmitted vortices are 100% of $l = 1$ for incident vortices with $l_i^b = 1$ and $l_i^b = -1$ (② and ④ procedures); the proportions are 33.3% ($T = T_a R_a = 0.25$) of $l = 1$ and 66.7% ($T = T_a = 0.5$) of $l = -1$ for

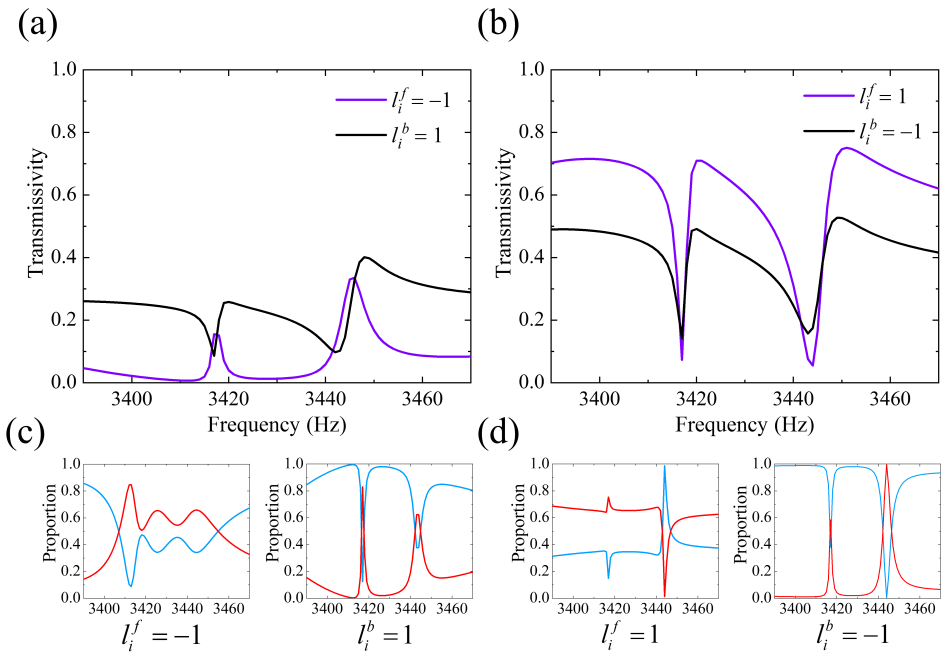


FIG. S3. Asymmetric transmission for the mirror-symmetric incidences. (a) and (b) The transmissivities for the two pairs of incident vortices with $l_i^f = -1$, $l_i^b = 1$ and $l_i^f = 1$, $l_i^b = -1$, respectively. (c) and (d) The corresponding topological charge proportions of transmitted waves. Red and blue represent vortices with topological charges of $-1$ and 1.

incident vortex with $l_i^f = 1$ (③ procedure). The corresponding simulated topological charge proportions are shown in Figs. S3(c) and S3(d). Transmitted vortices mostly exhibit $l = 1$ for $l_i^b = 1$ and $l_i^b = -1$ while the proportion of $l = 1$ and $l = -1$ in the transmitted vortices for $l_i^f = 1$ is 65% and 35% around 3430 Hz, respectively. These results agree well with the theoretical prediction. In addition, the theoretical transmissivities of the coupled processes shown in ② and ③ procedures of Figs. 2(d) and 2(e) are both $T = T_a R_a = 0.25$, while the corresponding simulated results are 0.215 and 0.212, respectively. When we design the transmissivities of all unit cells to satisfy $T_a = 0.9$, transmissivities of the coupled processes (② and ③ procedures) can be modulated to $T = T_a R_a = 0.09$. The simulated transmissivities become 0.131 and 0.123. Although there are some slight deviations that are mainly caused by the scattering of walls and the 2D approximation of the fanlike resonator, the asymmetric transmission is clearly exhibited and validated via transmissivities and topological charge

proportions. These results further demonstrate the analysis of the TRPC mechanism.

### G. Numerical demonstration of vortex transmission with broken mirror symmetry in the waveguide via coiling-up space structures.

To demonstrate the generalizability of the proposed TRPC mechanism, the fanlike coiling-up space structures are employed as an example to build a new TRI PGM, as shown in Fig. S4(a). The radius of both the PGM and waveguide is designed as $R = 4$ cm, where the maximum mode of the waveguide is $l_M = 1$. The working wavelength is still $\lambda = 10$ cm. Similar to the TRI PGM constructed with fanlike resonators, the PGM designed here also comprises six fanlike unit cells, divided into two supercells with an angular width of $\theta_t = \theta_r = 180^\circ$. The azimuthal cross-section of the coiling-up space structure is shown in Fig. S4(b), where the number $n$, length $h_a$, and space $d_w$ of the blocks are designed to realize the required phase responses and transmissivities [4]. Each unit cell contains a coiling-up space section with $d_1 = 0.5\lambda$ and a perforated panel with $d_2 = 0.25\lambda$, where the aperture size $h_b$ is utilized to stabilize transmissivity. The same phase differences between adjacent unit cells are also designed as $\Delta\varphi_t = -2\pi/3$, $\Delta\varphi_r = 2\pi/3$ and $\Delta\varphi_{rB} = 0$ with intrinsic topological charges of $l_t^\xi = -2$, $l_r^\xi = 2$ and $l_{rB}^\xi = 0$, while the transmissivity of each unit cell is close to 0.5, leading to $T_a = R_a = 0.5$ [see Fig. S4(c)]. The corresponding geometric parameters are listed in Table S1. Considering mirror-symmetric incident vortices of $l_i^f = -1$ ($l_i^b = 1$) for forward (backward) direction, the maximum mode $l_M = 1$ still limits the direct transmission of vortices with $l_t^f = l_i^f + l_t^\xi = -3$ ($l_t^b = l_i^b - l_t^\xi = 3$), leading to TRPC, while the reflected vortices with $l_r^b = -(l_i^f + l_r^\xi) = -1$ ($l_r^f = -(l_i^b + l_{rB}^\xi) = -1$) are allowed. Compared to the same incident cases in Fig. 2(d), the topological charge conversion processes occurring here are the same. Thus, the same one-way transmission for mirror-symmetric incident vortices can also be achieved, as demonstrated by the simulated results in Fig. S4(d). The corresponding simulated transmissivities are 0.007 for $l_i^f = -1$ and 0.231 for $l_i^b = 1$, while the theoretical predictions are 0 for $l_i^f = -1$ and 0.25 for $l_i^b = 1$, which agree well with each other.

For another pair of mirror-symmetric incident vortices with $l_i^f = 1$ ($l_i^b = -1$), the topological charge conversion processes are the same with the cases in Fig. 2(e). Vortex transmission with different topological charges for mirror-symmetric incidences can be achieved, as shown

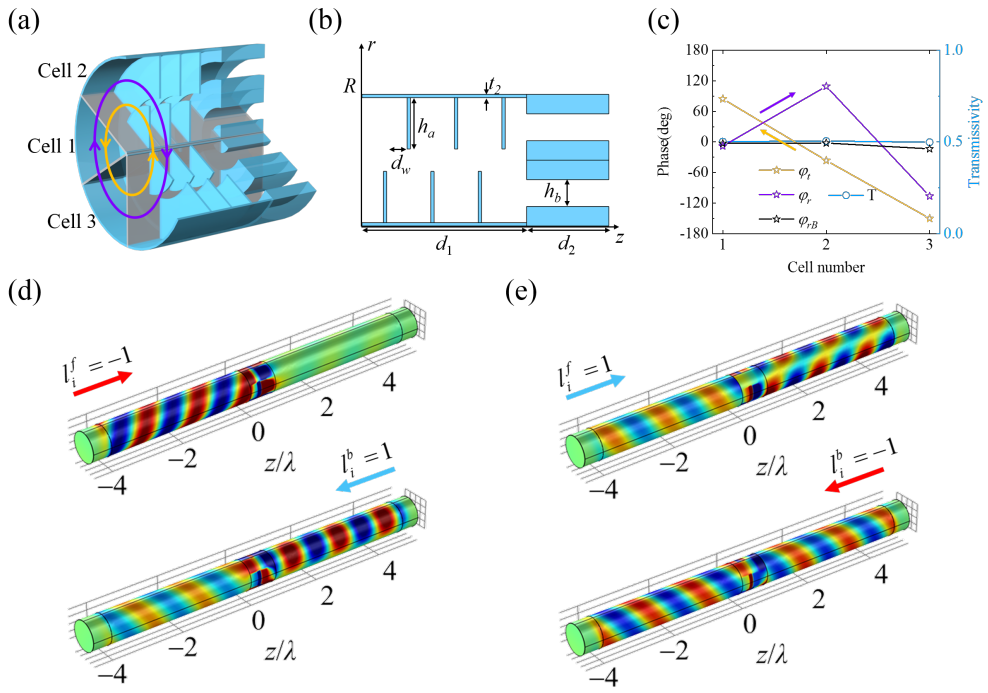


FIG. S4. Vortex transmission with broken mirror symmetry via coiling-up space structures. (a) Schematic diagram of the new TRI PGM, which is composed of six fanlike coiling-up space structures. (b) Azimuthal cross-section of a fanlike unit cell. (c) The simulated transmission and reflection phase responses and transmission spectra for each unit cell. (d) and (e) The simulated scattered pressure fields for two pairs of mirror-symmetric incident vortices at 3430 Hz, with the PGM placed at $z = 0$.

in Fig. S4(e). The simulated transmissivities are 0.782 for $l_i^f = 1$ and 0.554 for $l_i^b = -1$, while the theoretical results are 0.75 for $l_i^f = 1$ and 0.5 for $l_i^b = -1$ at 3430 Hz. In conclusion, the proposed TRPC mechanism exhibits the generalized physical principles applicable to different types of metasurfaces.

### H. Details of experiment.

A well-designed TRI PGM is placed in a 90-cm-long cylindrical waveguide and firmly sandwiched [see Fig. 4(a)]. An incident vortex with a topologic charge of $\pm 1$ can be excited by four circular speakers (2.5 cm diameter) with a phase of 0, $\pi/2$, $\pi$, $3\pi/2$ facing into the waveguide at one end. The speakers are wrapped in sound-absorbing cotton to reduce

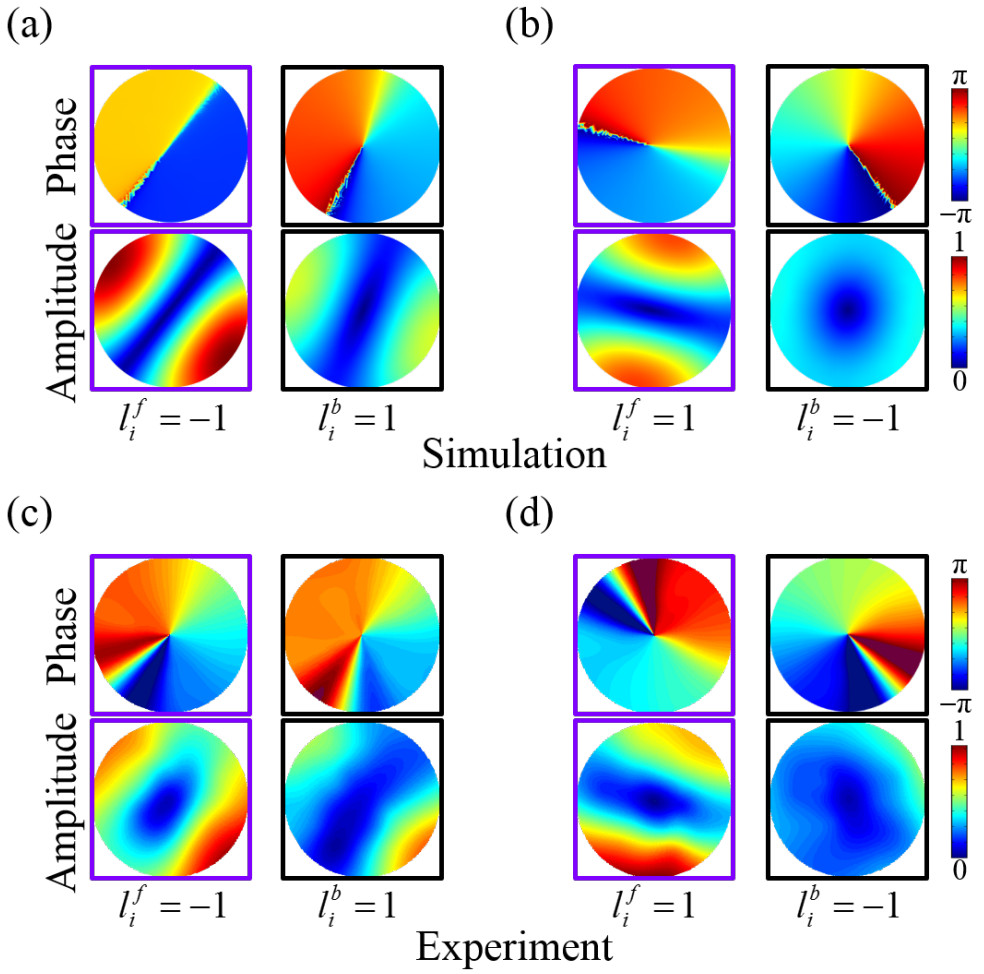


FIG. S5. Asymmetric reflection for the mirror-symmetric incidences. (a) and (b) The simulated amplitudes and phases of total pressure field patterns on the reflected sides of the forward and backward incidences. (c) and (d) The corresponding experimental results. The amplitudes are normalized by their maximum values.

undesired reflections from the source plane. The total acoustic field distributions of the transmitted and reflected waves are scanned using one microphone (B&K 4961, 1/4-inch diameter) with an angular width of 30° and a step of 2.0 cm. A Tektronix TBS 2000 series digital oscilloscope is employed to extract the amplitude and phase of the measured sound signal.

For the incident cases with $l_i^f = \pm 1$ and $l_i^b = \pm 1$, the simulated phase and amplitude distributions of total pressure field patterns for reflection at $z = -2.6\lambda$ and $z = 3.35\lambda$ are shown in Figs. S5(a) and S5(b), respectively. The corresponding experimental results

TABLE S1. Parameters of each unit cell.

| Parameter | $n$ | $h_a$ | $d_w$ | $h_b$ | $t_2$ |
|---|---|---|---|---|---|
| Cell 1 | 4 | $0.019\lambda$ | $0.055\lambda$ | $0.082\lambda$ | $0.01\lambda$ |
| Cell 2 | 4 | $0.167\lambda$ | $0.033\lambda$ | $0.06\lambda$ | $0.01\lambda$ |
| Cell 3 | 6 | $0.177\lambda$ | $0.043\lambda$ | $0.077\lambda$ | $0.01\lambda$ |

measured at the same positions are displayed in Figs. S5(c) and S5(d), respectively, which prove the theoretical analysis.


[1] J. F. Li, C. Shen, A. Diaz-Rubio, S. A. Tretyakov, and S. A. Cummer, Systematic design and experimental demonstration of bianisotropic metasurfaces for scattering-free manipulation of acoustic wavefronts, Nat. Commun. 9, 1342 (2018).

[2] Y. Tian, Q. Wei, Y. Cheng, and X. J. Liu, Acoustic holography based on composite metasurface with decoupled modulation of phase and amplitude, Appl. Phys. Lett. 110, 191901 (2017).

[3] S. Y. Zuo, Y. Tian, Q. Wei, Y. Cheng, and X. J. Liu, Acoustic analog computing based on a reflective metasurface with decoupled modulation of phase and amplitude, J. Appl. Phys. 123, 091704 (2018).

[4] Y. Y. Fu, Y. Tian, X. Li, S. L. Yang, Y. W. Liu, Y. D. Xu, and M. H. Lu, Asymmetric Generation of Acoustic Vortex Using Dual-Layer Metasurfaces, Phys. Rev. Lett. 128, 104501 (2022).